Combust. Sci. and Tech., 179: 1605–1630, 2007

ISSN: 0010-2202 print/1563-521X online
DOI: 10.1080/00102200701244710

Taylor & Francis
Taylor & Francis Group

Analysis of the Turbulent, Non-Premixed Combustion of Natural Gas in a Cylindrical Chamber with and without Thermal Radiation

C. V. Silva, F. H. R. França, and H. A. Vielmo*
Department of Mechanical Engineering,
Federal University of Rio Grande do Sul, Porto Alegre, RS, Brazil

Abstract: This work presents a numerical simulation of the non-premixed combustion of natural gas in atmospheric air in an axis-symmetric cylindrical chamber, focusing on the effect of thermal radiation on the temperature and chemical species concentration fields and the heat transfer. The simulation is based on the solution of the mass, energy, momentum and the chemical species conservation equations. Thermal radiation exchanges in the combustion chamber is computed through the zonal method, and the gas absorption coefficient dependence on the wavelength is resolved by the weighted-sum-of-gray-gases model. The turbulence is modeled by the standard $k - \varepsilon$ model, and the chemical reactions are described by the E–A (Eddy Breakup–Arrhenius model). The finite volume method is employed to treat the differential equations. Among other results, the solution of the governing equations allows the determination of the region where combustion takes place, the distribution of the chemical species, the velocity fields and the heat transfer rate by convection and radiation. The results indicate that while thermal radiation has a strong effect on the temperature field and heat transfer, its effect on the chemical reactions rates is of less importance. The numerical results are compared to experimental results obtained by Garréton and Simonin (1994).

Keywords: Arrhenius model; Eddy Breakup; Finite volume method; Heat transfer; $k - \varepsilon$ model; WSGGM model; Zonal method

Received 2 June 2006; accepted 26 January 2007.
The authors thank the financial support from CNPq-Brazil through a doctorate scholarship grant.
*Address correspondence to vielmoh@mechanica.ufrgs.bg

INTRODUCTION

An efficient operation of combustion chambers depends on the knowledge of the oxidation reactions and heat transfer between the combustion products and the chamber walls, which requires a detailed analysis of the governing mechanisms. A number of combustion modeling methodologies are now available, but only a few are able to account the process in its entirety. Eaton et al. (1999) present a revision of combustion models. The models are generally based on the fundamental conservation equations of mass, energy, chemical species and momentum, while the problem closure is achieved by turbulence models such as the $k-\varepsilon$ (Launder and Spalding, 1972; Launder and Sharma, 1974), combustion models like Arrhenius (Kuo, 1996; Fluent, 1997), Magnussen—EBU—"Eddy Break-up" (Magnussen and Hjertager, 1976), and radiative transfer models based on the radiative transfer equation (Özisik, 1985; Carvalho et al., 1991).

In a numerical investigation, Magel et al. (1996a) studied a 600 kW power cylindrical combustion chamber having a single burner located in the symmetry line. The eddy dissipation concept (EDC) combustion model, coupled to the $k-\varepsilon$ turbulence model, was employed to find the temperature, and the concentrations of oxygen, carbon monoxide and carbon dioxide at various locations in the chamber. Considering the same geometry and conditions, Magel et al. (1996b) performed a detailed analysis of the non-premixed turbulent combustion process, considering that the products were a gray gas with an absorption coefficient of $0.5\,\mathrm{m}^{-1}$ to solve the thermal radiation by the discrete ordinate method. In addition to the results such as above, they found the concentration of nitrogen oxide (NO) at different locations in the chamber.

Nieckele et al. (2001) employed the Fluent Inc. (1997) code to solve a similar problem as presented in Magel et al. (1996a). A number of combustion models were used, to mention the Arrhenius-Magnussen (E–A) and the so called PDFs (probability density functions) (Kuo, 1996; Fluent, 1997) models. Thermal radiation was solved by the discrete radiation model (DTRM) (Carvalho et al., 1991; Fluent Inc., 1997) using the WSGGM (Smith et al., 1982) to account the wavelength dependence of the gas radiative properties. The results obtained with the Arrhenius-Magnussen model showed the best agreement with the experimental data of Magel et al. (1996a).

Zhou et al. (2002) numerically investigated the formation of NO in turbulent combustion processes using the unified second-order moment (USM) model, based on the simultaneous solution of the conservation equations (mass, momentum, energy and chemical species) coupled to the standard $k-\varepsilon$ turbulence model, the equations of finite chemical reaction rates based on the Arrhenius laws and the assumption of a single global chemical reaction involving only two chemical species: oxygen and fuel.

It was analyzed the diffusion of methane and air free jet to predict the NO formation. The results presented a satisfactory agreement with experimental data and with results obtained with other combustion models, such as the E–A and the pre-PDF models. In a following work, Zhou et al. (2003) considered diffusive combustion of a jet of methane in air, without premixture. The USM model was again used to analyze the formation of NO for different swirl numbers. The USM model presented better agreement with the experimental data than the E–A and PDF models.

Fairweather and Woolley (2004) employed the first-order conditional moment closure (CMC) model to simulate the oxidation of methane free jet in turbulent, non-premixed flames, using the finite volumes discretization scheme. Turbulence was solved through the $k - \varepsilon$ and the Reynolds stress models, while the chemical reactions were tackled with two chemical kinetics schemes from the CHEMKIN library: the GRI-Mech 2.11 with 279 reactions and 49 species; and the GRI-Mech 3.0 with 325 reactions and 53 species. A number of simulations were carried out to demonstrate the efficiency and accessibility of the schemes. The results for the two turbulent flow models presented a good comparison with experimental data, with exception of the NO concentrations.

Guo et al. (2003) proposed a variation of the pre-PDF model, namely the joint-PDF model, for the solution of the average rates of the chemical reactions. In this model, the turbulent fluctuations of the reactants concentration and of the temperature are described, respectively, by pre-PDF functions based on tridimensional Gaussian distributions of first and second order. This model was applied to predict turbulent premixed combustion of methane/air in sudden-expansion flow and diffusive turbulent jet. Results of this model are compared to experimental data for pre-mixture flames and to results obtained with the β-PDF, E–A and the laminar Flamelet models. Both the join-PDF and the laminar Flamelet presented favorable comparisons.

Miroslav et al. (2001) carried out a numerical and experimental investigation of combustion of methane in air occurring in two coaxial turbulent streams. It was prescribed that a stoichiometric mixture of fuel and air was injected through a central orifice while pure air was inject by an outer annular orifice, so that both premixing and diffusion (non-premixed) existed. A second-order closure model for the Reynolds stress, which takes into account the turbulent stresses and the rate of turbulent kinetic energy dissipation, as well as the E–A combustion model were used. Since a single global chemical reaction was assumed, the chemical species conservation equations considered only methane (CH_4), oxygen (O_2), water vapor (H_2O), carbon dioxide (CO_2) and nitrogen (N_2). The obtained results presented a good agreement with the experimental data.

Malikov et al. (2002) performed a numerical analysis of combustion methane in air within a combustion chamber using a CFD code to solve

for the flow, temperature and chemical species concentration fields. The developed modeling is based on separate calculations of prompt and thermal NOx: the thermal NOx is calculated with the Zeldovich model; the prompt NOx is considered to be independent of the residence time and is computed with detailed kinetic data based GRI-Mech version 2.11 and CHEMKIN code by assuming that every computational cell were a perfectly stirred reactor. Three main parameters were considered to be critical in NOx production: (1) air equivalence ratio, (2) temperature, and (3) mixture dilution with combustion products. Comparisons of the model predictions with measurements were made for a wide range of industrial natural gas-fired burners installed in combustion chambers and furnaces.

Yang and Blasiak (2004) performed a numerical analysis of the effect of the temperature on the combustion process of a pre-heated, non-premixed jet of propane and air in a rectangular chamber. The modeling was based on the average conservation equations of energy, momentum and chemical species. Two combustion models were employed: the eddy breakup (EBU) and the PDF with β-function. The $k - \varepsilon$–RNG model was chosen to solve the turbulence effects, while the NO emission was solved by the NO thermal and the NO prompt models. Comparisons with experimental data proved favorable to the EBU model, especially with respect to the temperatures magnitudes and flame shape.

Finally, Salvador et al. (2006) carried out a numerical investigation of the combustion processes occurring inside the combustion chamber of a thermal recuperative incinerator (TIR) using the commercial Computational Fluid Dynamics (CFD) software, Fluent. The model was developed to simulate a combustion process of a mixture of natural gas diluted in atmospheric air flow. The coupled equations for flow, heat transfer, mass transfer and progress of chemical reactions were solved. The combined model of Eddy-Breakup–Arrhenius was used to solve the chemical reactions, while turbulence was simulated with the $k - \varepsilon$ model. Radiation heat transfer was not taken into account. Confrontation with experimental data was performed using a half-industrial-scale pilot unit.

The present work presents a numerical simulation of turbulent, non-premixed combustion of methane in air, involving two global steps of chemicals reactions, inside a cylindrical chamber that is similar to the one described in Garréton and Simonin (1994), for validation of the proposed solution. The finite volume method was used for the solution of the conservation equations of mass, momentum, energy and the main chemical species involved in the combustion process. The Eddy Breakup–Arrhenius (E–A) model (Fluent, 1997; Kuo, 1996; Magnussen and Hjertager, 1976; Turns, 2000) was employed to determine the reaction rates of the chemical species. To tackle the turbulence effects, the governing equations were time-averaged and the standard $k - \varepsilon$ model was used

for problem closure. Thermal radiation was computed by the zonal approach (Hottel and Sarofim, 1967; Siegel and Howell, 2002), with the direct-exchange areas being determined from relations provided in Sika (1992) for cylindrical geometry, together with the weighted-sum-of-gray-gases model (WSGGM) to account the wavelength dependence of the gas absorption coefficient. The weights and coefficients of the WSGGM model were taken from Smith et al. (1982) considering a gaseous mixture of H_2O, CO_2 and N_2, having partial pressures of 0.2, 0.1 and 0.7 atm, respectively, which is a typical composition of the products of the natural gas combustion. In reality, the concentrations of the chemical species in the chamber are non-homogeneous, and more sophisticated gas radiation models, such as those presented in Denison and Webb (1995) and Modest (2002), are necessary. However, those models impose an even more intense computational effort, and in fact have been applied mainly to one-dimensional systems with known temperature and chemical species concentrations. The WSGG model based on uniform species concentrations, despite its limitation, allows an averaged evaluation of the medium emission and absorption, at the same time that it can be integrated into a multi-mode computational model of combustion processes.

The combustion process in this case involves a number of very complex phenomena such as chemical reactions in the presence of turbulent flow, heat transfer by convection and radiation in participating media. Numerical simulations require the use of models for each one of these processes and the verification of the many models is still an on-going research. The majority of the works in the literature focus mainly on the chemical reactions, while the heat transfer by radiation is solved in less detail or is even neglected in the analysis. In the present work, the effect of thermal radiation is analyzed to serve as an indication of the errors that may occur when this heat transfer mechanism is not properly taken into account.

Mathematical Formulation

The proposed task can be stated as follows: considering steady combustion of methane in air, for a cylindrical chamber, compute the temperature, chemical species concentrations and the velocity fields, and verify the influence of the thermal radiation on the process.

As a basic assumption, it is considered that the combustion process occurs at finite rates with the methane oxidation taking two global steps according to Eq. (1), given by:

$$\begin{aligned} 2CH_4^{(16)} + 3(O_2^{(32)} + 3.76N_2^{(28)}) &\longrightarrow 2CO^{(28)} + 4H_2O^{(18)} + 11.28N_2^{(28)} \\ 2CO^{(28)} + 1(O_2^{(32)} + 3.76N_2^{(28)}) &\longrightarrow 2CO_2^{(44)} + 3.76N_2^{(28)} \end{aligned} \tag{1}$$

Mass Conservation

For cylindrical coordinates and taking advantage of axissymmetry, the continuity equation can be written as:

$$\frac{\partial}{\partial x}(\rho\bar{u}) + \frac{\partial}{\partial r}(\rho\bar{v}) + \frac{\rho\bar{v}}{r} = 0 \tag{2}$$

where x and r are the axial and radial coordinates, $\bar{u}$ and $\bar{v}$ are the time-average velocities in these respective directions and ρ is the specific mass of the gaseous mixture.

Momentum Conservation in the Axial ($\bar{u}$) and Radial ($\bar{v}$) Directions

The fluid flow equations are given by:

$$\begin{aligned}\bar{u}\frac{\partial}{\partial x}(\rho\bar{u}) + \bar{v}\frac{\partial}{\partial r}(\rho\bar{u}) = &-\frac{\partial p^*}{\partial x} + \vec{\nabla}\bullet((\mu+\mu_t)\vec{\nabla}\bar{u}) \\ &+ \frac{\partial}{\partial x}\left(\mu_t\frac{\partial\bar{u}}{\partial x}\right) + \frac{1}{r}\frac{\partial}{\partial r}\left(r\mu_t\frac{\partial\bar{v}}{\partial x}\right)\end{aligned} \tag{3}$$

$$\begin{aligned}\bar{u}\frac{\partial}{\partial x}(\rho\bar{v}) + \bar{v}\frac{\partial}{\partial r}(\rho\bar{v}) = &-\frac{\partial p^*}{\partial r} + \vec{\nabla}\bullet\left((\mu+\mu_t)\vec{\nabla}\bar{v}\right) + \frac{\partial}{\partial x}\left(r\mu_t\frac{\partial\bar{u}}{\partial r}\right) \\ &+ \frac{1}{r}\frac{\partial}{\partial r}\left(r\mu_t\frac{\partial\bar{v}}{\partial r}\right) - \frac{(\mu+\mu_t)\bar{v}}{r^2} + \frac{\rho\bar{w}^2}{r}\end{aligned} \tag{4}$$

where μ is the gaseous mixture dynamic viscosity and μ_t is the turbulent viscosity, defined as $\mu_t = C_\mu\rho k^2/\varepsilon$. The term $p^* = \bar{p} - (2/3)k$ is the modified pressure, C_μ is an empirical constant of the turbulence model, $\bar{p}$ is the time-averaged pressure of the gaseous mixture, and k and ε are the turbulent kinetic energy and its dissipation.

The $k-\varepsilon$ Turbulence Model

The equations for k and ε are:

$$\bar{u}\frac{\partial}{\partial x}(\rho k) + \bar{v}\frac{\partial}{\partial r}(\rho k) = \vec{\nabla}\bullet\left(\left(\mu+\frac{\mu_t}{\sigma_k}\right)\vec{\nabla}k\right) + P_k - \rho\varepsilon \tag{5}$$

$$\bar{u}\frac{\partial}{\partial x}(\rho\varepsilon) + \bar{v}\frac{\partial}{\partial r}(\rho\varepsilon) = \vec{\nabla}\bullet\left(\left(\mu+\frac{\mu_t}{\sigma_\varepsilon}\right)\vec{\nabla}\varepsilon\right) + C_{1,\varepsilon}\frac{\varepsilon}{k}P_k - C_{2,\varepsilon}\frac{\varepsilon^2}{k} \tag{6}$$

where $C_{1,\varepsilon}$ and $C_{2,\varepsilon}$ are empirical constants of the turbulence model, σ_k and σ_ε are the Prandtl numbers of the kinetic energy and dissipation,

respectively, and P_k is the production or destruction of the turbulent kinetic energy, given by:

$$P_k = \mu_t \left(2\left(\frac{\partial \bar{u}}{\partial x}\right)^2 + \left(\frac{\partial \bar{u}}{\partial r} + \frac{\partial \bar{v}}{\partial x}\right)^2 \right) + \mu_t \left(2\left(\frac{\partial \bar{v}}{\partial r}\right)^2 + 2\left(\frac{\bar{v}}{r}\right)^2 \right) \tag{7}$$

The E–A (Eddy Breakup–Arrhenius) Chemical Reactions Model

Chemical Species Conservation. The reduced chemical reactions model that is employed here assumes finite rate reactions and steady state turbulent process. In addition, it is considered that the non-premixed oxidation occurs in two global chemical reactions steps, and involving only six species: oxygen, methane, nitrogen, water vapor, carbon dioxide and carbon monoxide. A conservation equation is required for each species, with the exception of nitrogen. Thus, assuming a Lewis number ($Le = Sc_t/Pr_t$) of 1.0, one has the following conservation equation for the α-th chemical species:

$$\bar{u}\frac{\partial}{\partial x}(\rho \overline{f_\alpha}) + \bar{v}\frac{\partial}{\partial r}(\rho \overline{f_\alpha}) = \vec{\nabla} \bullet \left(\left(\rho D + \frac{\mu_t}{Sc_t} \right) \vec{\nabla} \overline{f_\alpha} \right) + \overline{R_\alpha} \tag{8}$$

where D is the mixture mass diffusivity, Sc_t is the Schmidt turbulent number, $\overline{f_\alpha}$ is the average mass fraction of the α-th chemical specie, and $\overline{R_\alpha}$ is the average volumetric rate of formation or destruction of the α-th chemical specie. This term is computed from the summation of the volumetric rates of formation or destruction in all the k-th equations where the α-th species is present, $\overline{R_{\alpha,k}}$. Thus, $\overline{R_\alpha} = \sum_k \overline{R_{\alpha,k}}$.

The rate of formation or destruction, $\overline{R_{\alpha,k}}$, can be obtained from an Arrhenius kinetic rate relation, which takes into account the turbulence effect, such as Magnussen's equations (Eddy Breakup) (Magnussen and Hjertager, 1976), or a combination of the two formulations, the so called Arrhenius-Magnussen's model (Eaton et al., 1999; Fluent Inc., 1997). Such relations are capable of dealing with a wide range of applications, for instance, laminar or turbulent chemical reactions with or without pre-mixing. Arrhenius's equation can be written as follows:

$$\overline{R_{\alpha,k,Chemical}} = -\eta_{\alpha,k} \overline{MM}_\alpha T^{\beta_k} A_k \Pi_\alpha C_\alpha^{\gamma_{\alpha,k}} \exp\left(\frac{-E_k}{\overline{R}T} \right) \tag{9}$$

where β_k is the temperature exponent in each chemical reaction k, which is obtained empirically together with the energy activation E_k and the coefficient A_k. Π_α is the product symbol, C_α is the molar concentration of the α-th reacting chemical specie, $\gamma_{\alpha,k}$ is the concentration exponent in each reaction k, $\overline{R}$ is the gas constant, $\overline{MM}_\alpha$ and $\eta_{\alpha,k}$ are the molecular mass and the stoichiometric coefficient of α in the k-th chemical reaction.

In the Eddy-Breakup or Magnussen's model, the chemical reactions rate are based on the theories of vortex dissipation in the presence of turbulence. Thus, for diffusive flames:

$$\overline{R_{\alpha,k,EBU}} = -\eta_{\alpha,k}\overline{MM}_{\alpha}K_1\rho\frac{\varepsilon}{k}\frac{\overline{f_{a^*}}}{\eta_{a^*,k}\overline{MM}_{\alpha^*}} \tag{10}$$

where the index α^* represents the reactant α that has the least value of $\overline{R_{\alpha,k,EBU}}$.

In the presence of premixing, a third relation for the Eddy Breakup model is necessary, so that

$$\overline{R_{\alpha,k,Premixing}} = \eta_{\alpha,k}\overline{MM}_{\alpha}K_1K_2\rho\frac{\varepsilon}{k}\frac{\sum_p\overline{f_p}}{\sum_p\eta_{p,k}\overline{MM}_p} \tag{11}$$

where the index p represents the gaseous products of the combustion. K_1 and K_2 are empirical constants that are set as 4 and 0.5 (Magnussen and Hjertager, 1976). Magnussen's model, Eqs. (10) and (11), can be applied to both diffusive and pre-mixed flames, or for the situation where both flames coexist, taking the smallest rate of chemical reaction.

Finally, for the Arrhenius-Magnussen's model, given by Eqs. (9)–(11), the rate of formation or destruction of the chemical species are taken as the least one between the values obtained from each model. It follows that

$$\overline{R_{\alpha,k}} = \min\left(\overline{R_{\alpha,k,Chemical}}, \overline{R_{\alpha,k,EBU}}, \overline{R_{\alpha,k,\ Premixed}}\right) \tag{12}$$

Observing the equations from the Eddy Breakup model, one verifies that the rates of chemical reactions are sensitive to the turbulent field, since the quantity ε/k, which appears in those equations, is dependent on the turbulence. However, the effect of turbulence on the density is only indirectly considered, that is the density is computed, using the ideal-gas state equation, from the local temperature and chemical species concentrations, which in turn are obtained from the Reynolds' time-averaged equation. A direct dependence of the density on the turbulent field can be accomplished by using the Favre's time-averaged equation or the weighted-density equation.

Energy Conservation. Neglecting the transport of energy due to the diffusion of each chemical specie, $Le = 1$, the energy equation can be written as

$$\overline{u}\frac{\partial}{\partial x}\left(\rho\bar{h}\right) + \bar{v}\frac{\partial}{\partial r}\left(\rho\bar{h}\right) = \vec{\nabla}\cdot\left(\left(\frac{\kappa}{c_p} + \frac{\mu_t}{Pr_t}\right)\vec{\nabla}\bar{h}\right) + \overline{S}_{rad} + \overline{S}_{rea} \tag{13}$$

where $\bar{h}$ and c_p are the average enthalpy and specific heat of the mixture. The latter is given by

$$c_p = \sum_{\alpha} \overline{f_\alpha} c_{p,\alpha} \tag{14}$$

where $c_{p,\alpha}$ and $\overline{f_\alpha}$ are the specific heat and the average mass fraction of the α-th chemical specie, κ is the thermal conductivity of the mixture, Pr_t is the turbulent Prandtl number, and $\overline{S}_{rad}$ and $\overline{S}_{rea}$ represent the sources of thermal energy due to the radiative transfer and to the chemical reactions. The term $\overline{S}_{rea}$ can be written as:

$$\overline{S}_{rea} = \sum_{\alpha} \left[\frac{h_\alpha^0}{\overline{MM}_\alpha} + \int_{\overline{T}_{ref,\alpha}}^{\overline{T}} c_{p,\alpha} d\overline{T} \right] \overline{R_\alpha} \tag{15}$$

where $\overline{T}$ is the average temperature of the mixture, h_α^0 and $\overline{T}_{ref,\alpha}$ are the formation enthalpy and the reference temperature of the α-th chemical specie.

To complete the model, the mixture specific heat can be obtained from the ideal gas state equation (Fluent, 1997; Kuo, 1996; Turns, 2000), $\rho = p\overline{MM}(\overline{R}\,\overline{T})^{-1}$, where p is the combustion chamber operational pressure, which is here set equal to 1 atm (Spalding, 1979), and $\overline{MM}$ is the mixture molecular mass.

The aforementioned equations are valid only in the turbulent core, where $\mu_t \gg \mu$. Close to the wall, the viscous region, the law of the wall is used. For the numerical simulation, this law is applied in the region between the wall and the first nodal grid point. In this way, a linear velocity is applied in the region close to the wall, while a logarithmic profile is taken in the fully turbulent region, so that

$$\begin{aligned} y^+ \leq 11,5 &\rightarrow u^+ = y^+ \\ y^+ > 11,5 &\rightarrow u^+ = (1/\mathrm{A})\ln(y^+) + \Psi \end{aligned} \tag{16}$$

where $y^+ = y\left(\rho C_\mu^{1/4} k^{1/2} \mu^{-1}\right)$ is a dimensionless distance from the wall, $u^+ = \bar{u}/u^*$ is a dimensionless velocity, $u^* = \sqrt{\tau_w/\rho}$ is the friction velocity, in which τ_w is the shear stress on the wall, and y is the distance from the wall. According to Nikuradse (1933): $\mathrm{A} = 0.4$ and $\Psi = 5.5$. The condition of equilibrium between production and destruction of turbulent kinetic energy together with the assumption of constant shear stress in the viscous region leads to kinetic energy gradient null on the wall, so

$$\varepsilon = C_\mu^{3/4} k^{3/2} (\mathrm{A}y)^{-1} \tag{17}$$

To account thermal radiation exchanges inside the combustion chamber, the zonal method is employed (Hottel and Sarofim, 1967; Siegel and

Howell, 2002). The method consists of dividing the computational domain into finite-size zones in the gas and surfaces. Since the combustion of natural gas does not involve the presence of soot or other particulates, it can be assumed that the medium does not scatter thermal radiation. The effect of the wavelength dependence of the gas absorption coefficient is accounted by the weighted-sum-of-gray-gases-model (WSGGM). From this, it follows that the net radiative transfer rate per unit of volume in a gas zone is:

$$\overline{S}_{rad,\gamma} = -\frac{1}{V_\gamma}\left(\sum_i 4V_\gamma a_i \sigma \overline{T}_\gamma^4 - \sum_{\gamma^*=1}^{\Gamma} \overrightarrow{g_{\gamma^*} g_\gamma}\sigma \overline{T}_{\gamma^*}^4 - \sum_{j=1}^{J} \overrightarrow{s_j g_\gamma} q_{o,j}\right) \tag{18}$$

On the right-hand side, the first term is the energy emitted by the gas zone having volume of V_γ, while the second and the third terms account the rate of radiative energy that is absorbed by the gas zone that is originated from the other gas zones of volume V_{γ^*} and from other surface zones j. σ is the Stefan-Boltzmann constant, $\overrightarrow{g_{\gamma^*} g_\gamma}$ and $\overrightarrow{s_j g_\gamma}$ are the gas-to-gas and surface-to-gas directed-flux areas. $q_{o,j}$ is the outgoing radiative heat flux of surface j.

For a surface zone A_k, the net radiative heat transfer rate per unit of area is

$$\overline{S}_{rad,k} = \frac{1}{A_k}\left(\sum_{\gamma=1}^{\Gamma} \overrightarrow{g_\gamma s_k}\sigma \overline{T}_\gamma^4 + \sum_{j=1}^{J} \overrightarrow{s_j s_k} q_{o,j}\right) - q_{o,k} \tag{19}$$

where the first and the second terms on the right-hand side correspond to the radiative energy from the other gas zones V_γ, and from the surface zones k that reach surface zone j. $\overrightarrow{g_\gamma s_k}$ and $\overrightarrow{s_j s_k}$ are the gas-to-surface and surface-to-surface directed-flux areas. The direct-flux areas were obtained from the gray gases weights and absorption coefficients, as presented in Smith et al. (1982) for a gaseous mixture of H_2O, CO_2 and N_2 at 1.0 atm, and having partial pressures of 0.2, 0.1 and 0.7, respectively, and from the relations for direct-exchange areas, which are provided by Sika (1992) for cylindrical enclosures.

PROBLEM STATEMENT

The physical system consists of the same natural gas combustion chamber that was analyzed in Magel et al. (1996-a), which was a test case proposed in Garréton and Simonin (1994). The cylindrical chamber has a length and a diameter of 170 cm and 50 cm, respectively, as shown in Figure 1. Natural gas is injected into the chamber by a duct aligned with the chamber centerline. The burner is capable of providing the necessary

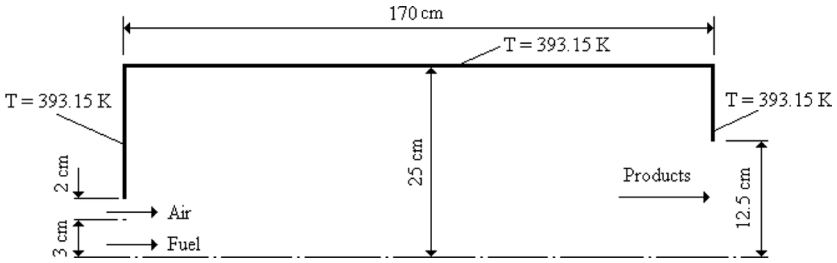

Figure 1. Combustion chamber geometry.

amount of air and natural gas as required by the process. In all cases a fuel excess of 5% was prescribed. For a fuel mass flow rate of 0.0125 kg/s at a temperature of 313.15 K, this requires an air mass flow rate of 0.186 kg/s, at a temperature of 323.15 K. The fuel enters the chamber through a cylindrical duct having diameter of 6 cm, while air enters the chamber through a centered annular duct having a spacing of 2 cm. For such mass flow rates, the fuel and air velocities are 7.76 and 36.29 m/s, respectively. The Reynolds numbers at the entrance points that the flow is turbulent (approximately 18000). The inlet air is composed of oxygen (23% in mass fraction), nitrogen (76%) and water vapor (1%), while the fuel is composed of 90% of methane and 10% of nitrogen. The burner power is about 600 kW.

The fan and the other external components are not included in the computational domain, although their effects are taken into account through the inlet flow conditions. Buoyancy effects are neglected due to the high velocities that are provided by the burner.

THERMOPHYSICAL PROPERTIES

The equations constants and the physical properties were taken from a number of different sources, and are presented in Table 1. It is assumed that all properties are constant for all the species (CH_4, O_2, H_2O, CO, CO_2 and N_2), with the exception of the specific heats that are used to determine the temperature.

Table 2 presents the temperature dependence of the specific heats at constant pressure for the different components. The specific heat of the mixture was obtained from a mass weighted average. The other thermophysical properties for the mixture were taken as those of the air, since it has the highest concentration.

For the chemical reaction of the methane ($k = 1$ in Eq. (1)), it was assumed that the values of the activation energy, $E_{k=1}$, and of the coefficients $A_{k=1}$ and $\beta_{k=1}$ in the Arrhenius equation were 2.03×10^8, 2.8×10^{12}

Table 1. Thermophysical properties that were used in the simulation

Property	Value	Property	Value
$\overline{MM}_{N_2}$ (kg/kmol)	28	$\overline{MM}_{CH_4}$ (kg/kmol)	16
$\overline{MM}_{CO_2}$ (kg/kmol)	44	$\overline{MM}_{H_2O}$ (kg/kmol)	18
$\overline{MM}_{CO}$ (kg/kmol)	28	$\overline{MM}_{O_2}$ (kg/kmol)	32
σ (W/m^{2}K^4)	5.6697×10^{-8}	μ (Ns/m^2)	2.97×10^{-5}
κ (W/mK)	45.4×10^{-3}	D (m^2/s)	2.88×10^{-5}
$\overline{\mathrm{R}}$ (kJ/kmolK)	8.3145	σ_k (−)	1.0
C_μ (−)	0.09	σ_ε (−)	1.3
$C_{2,\varepsilon}$ (−)	1.92	Sc_t (−)	0.9
$C_{1,\varepsilon}$ (−)	1.44	Pr_t (−)	0.9
$h^0_{CO_2}$(J/kg)	3.94×10^8	$h^0_{O_2}$(J/kg)	0
$h^0_{N_2}$(J/kg)	0	$h^0_{H_2O}$(J/kg)	2.42×10^8
h^0_{CO}(J/kg)	1.11×10^8	$h^0_{CH_4}$(J/kg)	7.49×10^7

and zero, respectively. It was also considered that the orders of the chemical reactions of methane, γ_{CH_4}, and of the oxygen, γ_{O_2}, were -0.3 and 1.3, respectively. For the chemical reaction of the carbon monoxide ($k = 2$ in Eq. (1)), the activation energy, $E_{k=2}$, and the coefficients $A_{k=2}$ and $\beta_{k=2}$ in the Arrhenius equation were set equal to 1.67×10^8, 2.91×10^{12} and zero, respectively. In addition, the orders of the chemical reactions of the carbon monoxide, γ_{CO}, and of the oxygen, γ_{O_2}, were taken as 0.25 and 1.0, respectively. The remaining coefficients for the chemical reactions orders were assumed equal to zero (Turns, 2000).

BOUNDARY CONDITIONS

Keeping the same conditions as prescribed in Garréton and Simonin (1994), the combustion chamber walls were kept at constant temperature

Table 2. Temperature dependence of the specific heats at constant pressure (Van Wylen et al., 2003)

Temperature (K)	c_{p,CH_4} (J/kgK)	c_{p,O_2} (J/kgK)	c_{p,N_2} (J/kgK)
300	2226	914	1045
600	3256	1005	1075
1000	4475	1084	1164
1500	5408	1360	1239
2000	5904	1175	1283
2500	6165	1215	1314

of 293.15 K. In addition, impermeability and no-slip conditions were assumed on the wall. In the symmetry line, it was assumed that both the radial velocity and the velocity gradient were null. In the outlet, null diffusive fluxes were assumed for all variables, the axial velocity component was corrected by a factor to satisfy mass conservation, and the radial velocity was imposed to be null. The walls were assumed gray, diffusive emitters with an emissivity of 0.6. The inlet and the outlet reservoirs were modeled as black surfaces at the inlet and outlet temperatures. While the first one was prescribed, the outlet temperature was equal to the outlet flow bulk temperature, $\overline{T}_{bulk}$, as given by:

$$\overline{T}_{bulk} = \frac{\int_A \rho u c_p T \, dA}{\int_A \rho u c_p \, dA} \tag{20}$$

In the inlet, the velocity and concentration profiles were assumed uniform. The kinetic turbulent energy was computed by $k = 3/2(\bar{u}_{in} I)^2$, where I is the turbulence intensity (prescribed as 6% and 10% for the air and the fuel flows, respectively) and $\bar{u}_{in}$ is the inlet axial velocity. For the turbulent kinetic dissipation, the relation $\varepsilon = C_\mu^{3/4} k^{3/2}/l$ was employed, where l is the turbulence characteristic length scale (taken as 0.04 m and 0.03 m for the air and the fuel flows, respectively).

NUMERICAL SOLUTION

The diffusive-advective interpolation function on the faces of the control volumes is the power-law. The pressure-velocity coupling is made by the SIMPLE method. Grid independence tests led to a mesh having 35 and 70 volumes in the radial and axial directions, respectively. Twenty-four out of the 35 volumes in the radial direction were distributed in the region between 0 and 12.5 cm, matching the sizes of the inlet and outlet ducts. Closer to the wall, ore refinement was applied to capture the boundary effects. In the axial direction, a uniform grid size was adopted to take advantage of the symmetry between the direct-exchange areas, and reduce the computation effort. This mesh proved adequate in the sense that it led to satisfactorily precise results without demanding excessive computational effort. A grid independence analysis is shown in Figure 2 for the temperature distribution along the axial position for a radius position of 12.5 cm. For other radial positions, a similar behavior was observed. For the solution of the radiative heat exchanges, the enclosure was divided into zones of volume and surface that had the same dimensions of the control volumes. The resulting system of algebraic equations was solved by the TDMA algorithm, with block correction in all equations but the k and ε equations.

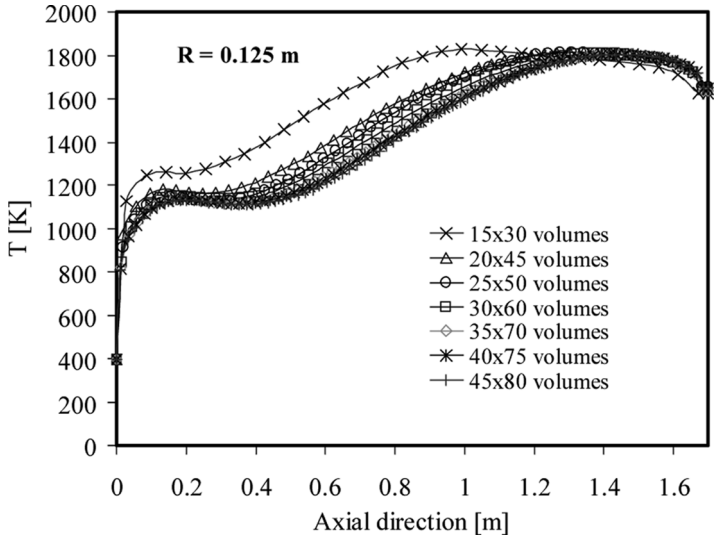

Figure 2. Grid independence test: temperature distribution along the axial direction for a radius of 0.125 m.

The general algorithm is now described. First, from the problem specification, the thermophysical properties were obtained and then the velocity and pressure fields were computed. Next, the enthalpy, chemical species concentration and turbulence equations were solved. For the solution of the energy equation, the radiative heat source was first assumed null. Once the temperature field was obtained from the enthalpy field, the radiative heat exchanges between the zones were computed from the zonal analysis and the weighted-sum-of-gray-gases model. This allowed the determination of the radiative heat source in the zones, which were then inserted into the energy equation. This iterative process was repeated until convergence is reached. Most of the source terms in the conservation equations were linearized and when necessary approximated by finite difference approximations. Due to its complexity, the radiation source term was explicitly computed from the temperature field obtained from a previous step solution of the energy equation.

The specific heat dependence with respect to the temperature, as illustrated in Table 2, was taken into account with the aid of the integral relations that are presented in Van Wylen et al. (2003).

Convergence criteria was based on the imposition that summation of the normalized residual of all the equations and of the enthalpy equation were less than 10^{-9} and 10^{-7}, respectively.

RESULTS ANALYSIS

The main goal of this investigation is the analysis of the effect of thermal radiation on the non-premixed combustion of natural gas in a cylindrical chamber. For this, it will be presented temperature fields, the heat transfer, and the chemical species concentration distributions when thermal radiation is considered (case 1) and not considered (case 2).

For a better understanding of the phenomenon, it is first considered the fluid flow velocity pattern. Figure 3a presents the streamline function in the chamber, showing the existence of a secondary recirculating flow occupying most of the chamber upper left part. This is due to the high velocities of the air and fuel jets in the chamber inlet, as depicted by the dark region between the recirculation region and the symmetry line. As a result of the fluid flow dynamics, a low pressure region is formed in the upper left corner, causing a flow inversion and the formation of a vortex that is sustained by the shear stress with the main flow.

Figure 3b presents the velocity field vectors in the chamber. For sake of comparison, the highest and the lowest velocities in the chamber are approximately 37 and 2 m/s, respectively. The results show that the highest velocities are found in the chamber core (the symmetry line) and towards the chamber exit, for two mains reasons: the decrease in the gaseous mixture density with the increase of the temperature and the decrease in the flow passage area. On the other hand, the lowest velocities are found in the recirculation region close to the chamber wall. The flow field results that are presented in Figures 3a and 3b were obtained for case 1, considering thermal radiation, but little difference was observed when it was neglected.

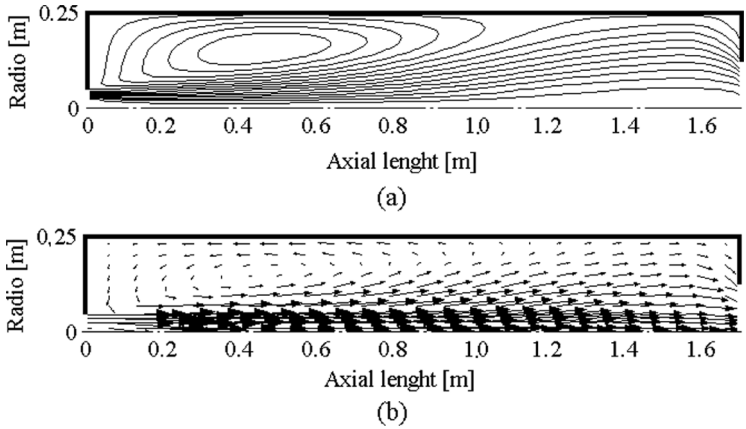

Figure 3. (a) Streamline function; (b) Velocity field vectors.

Figures 4a and 4b present, respectively, the temperature fields for cases 1 and 2. As can be seen, the maximum temperatures that were obtained for both cases were approximately 1750 K. On the other hand, when thermal radiation is taken into account, the temperature gradients in the chamber were decreased since this mechanism homogenizes the temperatures between the hot and cold regions of the chamber. For case 1, the highest temperatures are limited to a narrower region in the core of the chamber exit. Figure 4c, which presents the volumetric radiative heat source in the medium, corroborates the above observation. As seen, the

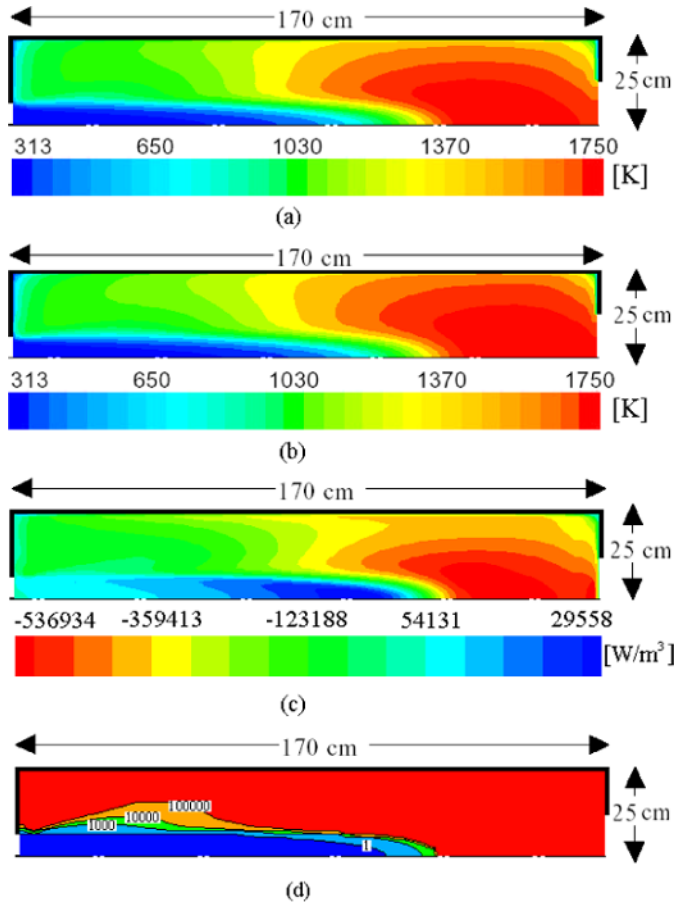

Figure 4. (a) Temperature distribution in the chamber considering thermal radiation (case 1); (b) Temperature distribution in the chamber without considering thermal radiation (case 2); (c) Volumetric radiative heat source distribution in the chamber; (d) Damköhler number field.

high temperature regions presents negative radiative heat source, since the amount of radiation energy received from the other regions of the chamber are less than the emitted energy. The contrary occurs in the low temperature regions, that is, the radiative heat source is positive. For case 2, shown Figure 4b, the heat transfer is governed mostly by advection of thermal in the flow direction. For this reason it cannot provide the heating of the low temperature regions in the chamber inlet by the high temperature regions in the chamber outlet, and one finds higher temperature gradients. A radiative energy conservation balance, which accounts the total amount of absorbed and emitted energy in all gas and wall zones in the chamber, led to a relative error of 0.89%.

Despite the aforementioned differences, the temperature fields obtained for the two cases present similar characteristics: that is, a cold jet in the core and hot gases occupying the regions around the centerline close to the chamber outlet. The explanation for the similar trends relies on the fact that the chemical energy heat source is the dominant mechanism that governs the temperature field. In fact, in the solution of Eq. (12), the combustion heat source proved to be much greater than the radiative heat source. One additional explanation arises from an inspection of the mechanisms that govern the chemical reactions, as will be discussed next.

Figure 4d presents the distribution of the Damköhler number, Da, which expresses the ratio between τ_t, the characteristic turbulence time, and τ_{ch}, the characteristic chemical reactions time, that is, $Da = \tau_t/\tau_{ch}$. When chemical reactions rates are fast in comparison with fluid mixing rates, then $Da \gg 1$, and a fast-chemistry regime is defined. On the other hand, when the chemical reactions rates are slow in comparison with mixing rates, then $Da \ll 1$ (Turns, 2000). Note that the characteristic rates are inversely proportional to their corresponding characteristic times. In other words, the Damköhler number can indicate the regions where the combustion process is governed by the chemical kinetics and by the fluid flow. Note that the Damköhler number can also be obtained from the ratio between the chemical reaction rates calculated from Eqs. (9) and (10), that is, $Da = \overline{R_{\alpha,k,Chemical}}/\overline{R_{\alpha,k,EBU}}$.

Four regions bounded by constant values of the Damköhler number, $Da = 1$, 1×10^3, 1×10^4 and 1×10^5 are presented. In the chamber core, which is occupied by the cold inlet jet, the combustion process is governed by the Arrhenius chemical reactions equation since $Da \ll 1$, while in all the other regions it is governed by the Eddy Breakup instantaneous chemical reactions equation. Since the Arrhenius equation is temperature dependent, in the inlet region the chemical reactions rate are the lowest leading to a gradual increase in the temperature up to a point where the gaseous mixture reach a temperature in which, with the aid of a more intense turbulence, the combustion rate is greatly

intensified. The observation of the temperature fields obtained for cases 1 and 2 (Figures 4a and 4b, respectively) reveals that the thermal radiation has only a minor effect on the core region, which is where the chemical reactions are temperature dependent and where most of the combustion process takes place.

Figure 5 presents a comparison between the temperature distribution along the chamber centerline obtained for cases 1 and 2. As seen, the temperature distributions are practically the same up to a distance of 1.3 m from the chamber inlet, where the temperature for the case 1 becomes smaller than that for case 2. For the regions located at a distance less than 1.3 m, the temperatures are relatively low, and so the effect of the thermal radiation is smaller. For positions downstream of 1.3 m, the temperatures are higher, and then the thermal radiation exchanges reduces the temperatures. On the other hand, it is not observed any effect of the inclusion of the thermal radiation on the concentrations of the fuel CH_4, the carbon dioxide, oxygen and carbon monoxide along the center line, as depicted in Figures 6a to 6d, respectively. This can be explained by the fact that thermal radiation exchanges has very little effect on the chemical

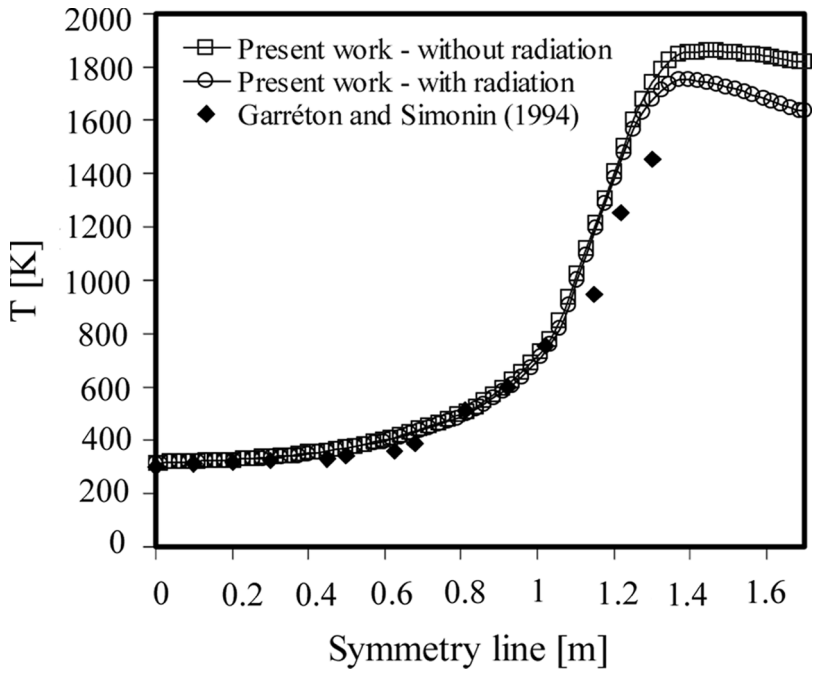

Figure 5. Temperature distributions along the symmetry line for cases 1, 2 and the experimental data (Garréton and Simonin, 1994).

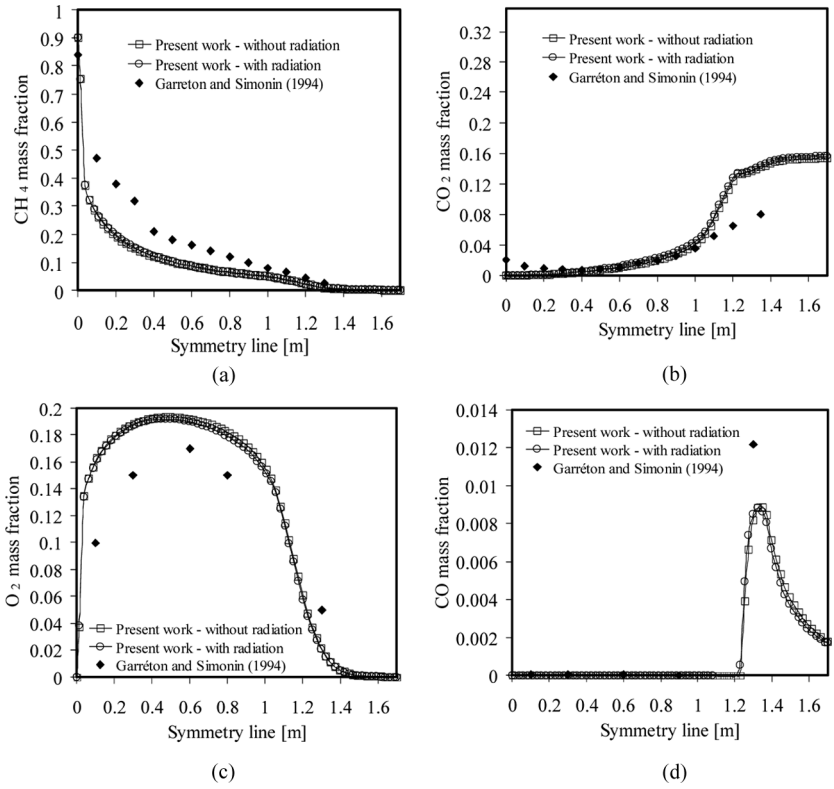

Figure 6. Chemical species concentrations along the symmetry line for cases 1, 2 and the experimental data (Garréton and Simonin, 1994): (a) fuel CH_4; (b) carbon dioxide; (c) oxygen; (d) carbon monoxide.

reactions on the chamber center line, since the temperature dependent reactions are mostly occurring in the cold core jet, which is unaffected by the presence of the radiative exchanges, as seen in Figures 4a and 4b. Figures 6a to 6d also include the data presented by Garréton and Simonin (1994). The results show that the predicted combustion products concentrations have trends that are similar to those of the experimental data.

Figures 7a to 7c present the temperature distribution along the radial position for three different locations for cases 1 and 2 and the experimental data of Garréton and Simonin (1994). The figures show that the inclusion of thermal radiation results in a reduction in the magnitude of the temperature. A difference of up to 160 K between the two solutions for cases 1 and 2 can be observed in some regions, especially in Figure 7c. As discussed previously, this reduction is related to the

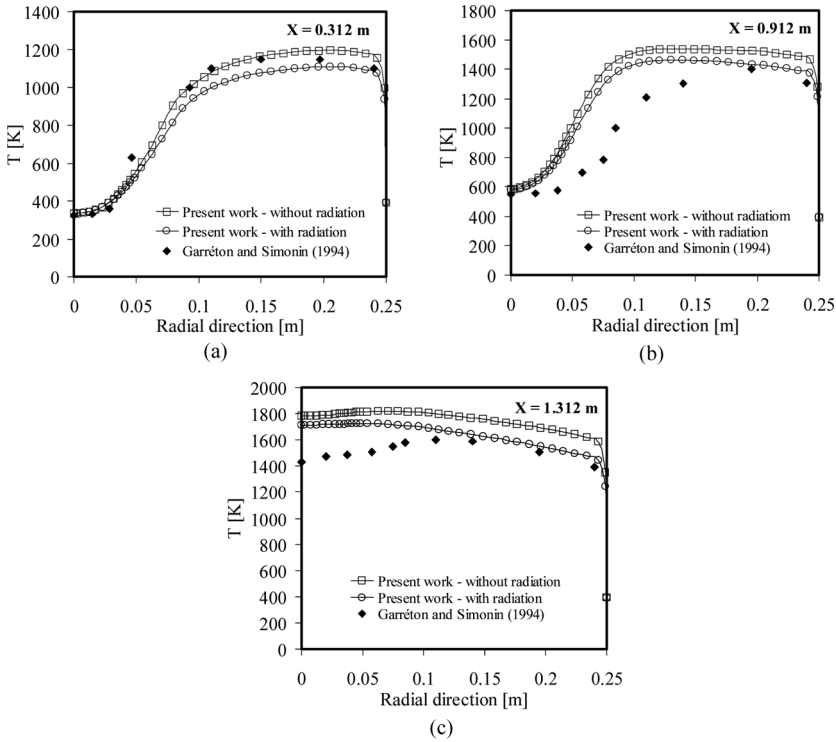

Figure 7. Effect of the thermal radiation on the temperature distributions along the radial position at: (a) 0.312 m from the entrance; (b) 0.912 m from the entrance; (c) 1.312 m from the entrance.

heat transfer by radiation from the high to the low temperature regions in the chamber. Observing Figures 7a to 7c, one also notes that the results for case 1, which considers thermal radiation, present a better comparison with the experimental data, mainly in the high temperature zones.

Figures 8a to 8c present the oxygen concentration along the radial positions at three different axial locations: 0.312, 0.912 and 1.312 m from the chamber inlet. As seen, there is a small elevation in the oxygen consumption (or, alternatively, there is a small decrease in the concentration) when thermal radiation is incorporated into the analysis. This is related to a change in the chemical reactions rate due to its dependence on the temperature. It can also be seen that the results obtained for the axial positions of 0.312 and 0.912 m follow the same trends of the experimental data, showing a good agreement. On the other hand, for an axial position of 1.312 m, there is not a good agreement. The numerical results predict a

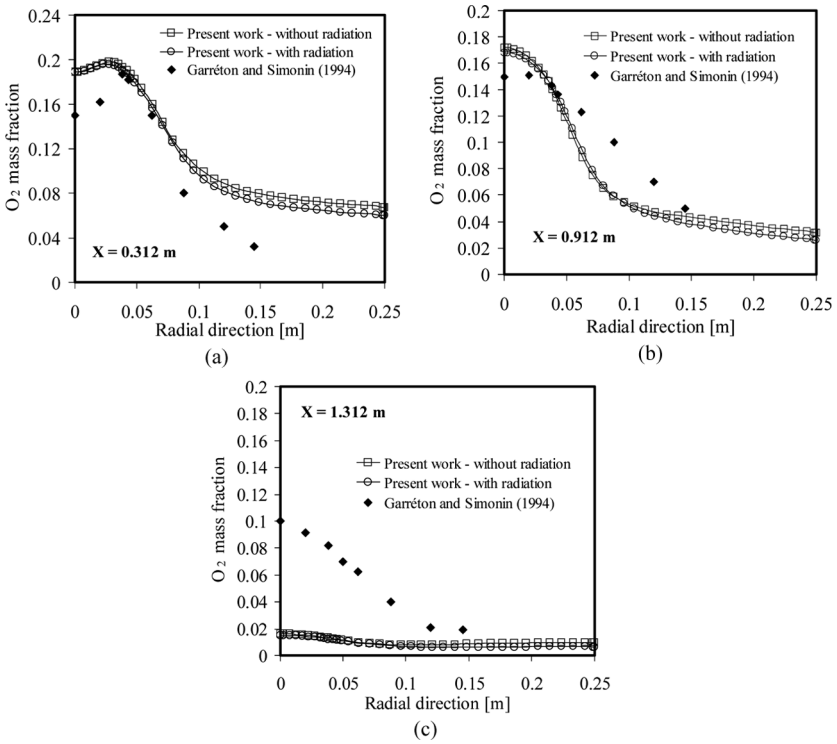

Figure 8. Effect of the thermal radiation on the oxygen concentration along the radial position at: (a) 0.312 m from the entrance; (b) 0.912 m from the entrance; (c) 1.312 m from the entrance.

combustion core of shorter length, so at the position of 1.312 m, little amount of oxygen is left.

In Figures 9a to 9c, it is considered the effect of thermal radiation on the concentration of CO_2 along the radial position for different axial positions. The figures show that the inclusion of thermal radiation leads to an increase in the CO_2 concentration for all the axial positions. This increase is associated with the increase in the consumption of oxygen in the chemical reactions, as seen in Figs. 8a to 8c. It is also observed that the numerical results show a similar trend of the experimental data, especially for the axial position of 0.312 m.

An additional view of the effect of thermal radiation is presented in Fig. 10, which shows the heat transfer to the chamber outside for cases 1 and 2. The inclusion of thermal radiation has a major effect in the heat transfer, which is given by the sum of the heat transfer by radiation and convection (also shown in the figure). Figure 10 indicates that the

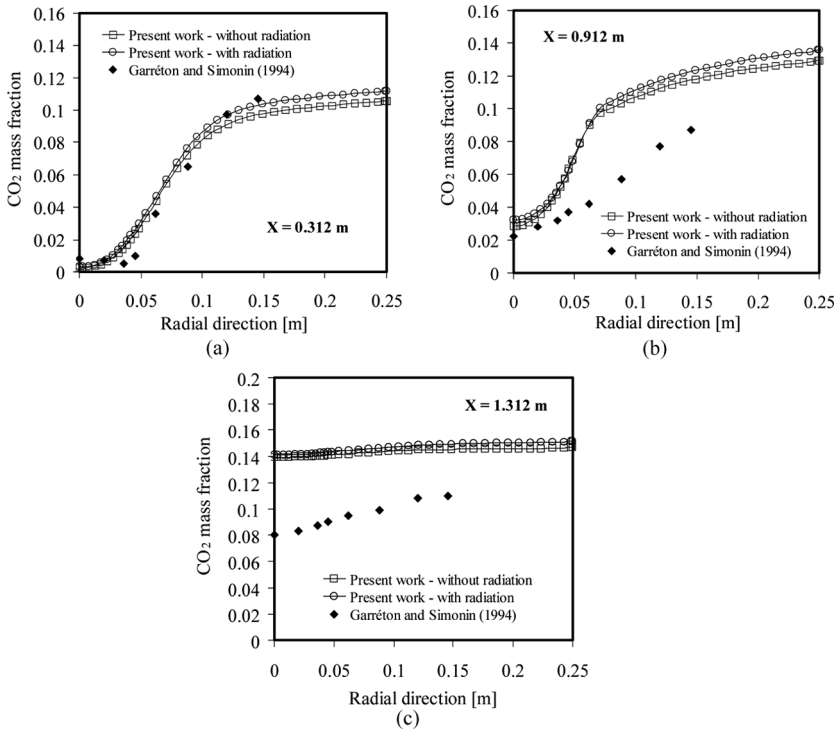

Figure 9. Effect of thermal radiation on the carbon dioxide concentration along the radial position at: (a) 0.312 m from the entrance; (b) 0.912 m from the entrance; (c) 1.312 m from the entrance.

thermal radiation is the dominant mechanism for most of the chamber length, with the exception of the inlet section. In the solution that neglects thermal radiation, the heat transfer is purely convective.

It is interesting noting that when thermal radiation is included, the convective heat transfer decreases in comparison to that when thermal radiation is neglected, since the temperature gradients in the chamber are reduced.

Finally, it is of interest to perform an energy balance in the chamber. For cases 1 and 2, the inlet energy inputs into the chamber are the same and includes: 8.42 kW for the fuel flow, related to the enthalpy of the fuel at 313.15 K; 65.24 kW for the air flow, related to the enthalpy of air at 323.15 K; and 561.33 kW that is related to the combustion enthalpy of the natural gas. Thus, the total energy input in the chamber is 635.19 kW.

For case 1, in which thermal radiation is considered, the energy output includes: 3.14 kW for the fuel flow that was not burnt; 455.91 kW for

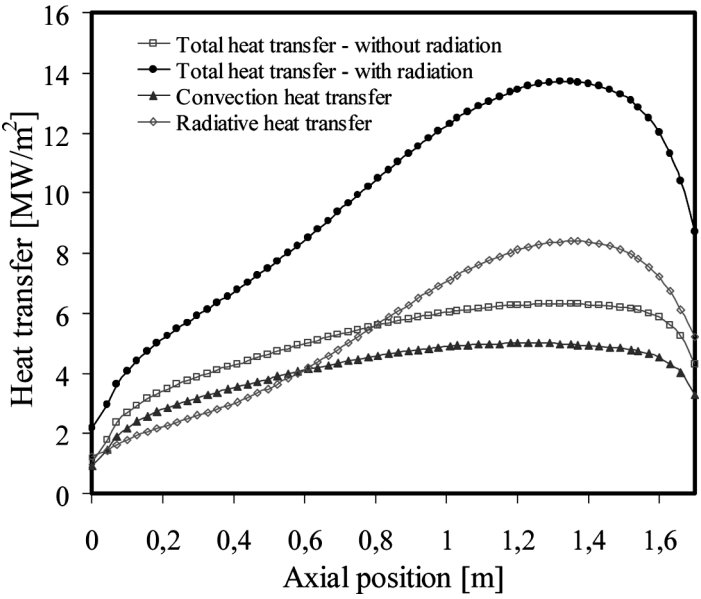

Figure 10. Heat transfer on the chamber wall when thermal radiation is considered (case 1) and when it is not considered (case 2).

the gaseous products; and 162.05 kW for the heat transfer to the chamber outside. This gives a total output of 621.10 kW, and the percentage of heat transfer to the chamber outside is equal to 26.09%. The error between the prescribed energy input and the computed energy output is 2.2%, which can be attributed to the numerical approximations.

The same can be done for the case 2, neglecting thermal radiation. The energy output includes: 2.73 kW for the fuel flow that was not burnt; 526.22 kW for the gaseous products; and 84.44 kW for the heat transfer to the chamber outside. This gives a total output of 613.39 kW. The percentage of heat transfer to the chamber outside is in this case 13.29%, which is half the value obtained when thermal radiation is included. The error between the prescribed energy input and the computed energy output for this case is 3.4%.

The combustion efficiencies obtained for cases 1 and 2 were 98.96% and 99.56%, respectively. The small difference is due to the fact that the inclusion of thermal radiation reduces the temperatures in the chamber, and so the rate of the chemical reactions is decreased, reducing the efficiency of the process. However, as depicted in the figures that show the effect of thermal radiation of the chemical species concentration, this effect is only minor.

CONCLUSIONS

The results presented in this work indicate that the major effect of thermal radiation was in the temperature field and heat transfer. The radiative exchanges caused a more effective homogenization of the temperatures inside the combustion chamber, reducing the peaks of temperature and increasing the lower temperatures. In some regions, it was observed a variation of 160 K in the temperatures obtained for the cases with and without thermal radiation. The inclusion of thermal radiation also led to an increase in the heat transfer from the hot gas to the chamber outside, predicting a value that was twice the one obtained without considering thermal radiation. In most of the chamber the heat transfer by radiation was more important than by convection. On the other hand, the effect of the thermal radiation on the chemical reactions rates proved less important, at least in the framework of the chemical reactions models employed in this investigation, although changes were observed in the concentrations of oxygen and carbon dioxide in some regions of the chamber. Since the radiative exchanges had a small effect on the temperature in the core jet, where most of the combustion takes place, its effect on the consumption of the chemical species was only marginal, resulting in nearly no change in the efficiency of the combustion process in comparison to the case without thermal radiation. A possible explanation for this is that, in general, the use of global chemistry predictions leads to steeper increases in temperature in addition to no radicals being calculated. An interesting next step in this research would be the use of more detailed chemistry models, which have the potential of bringing important new effects, mainly in the core region. In such models, the chemical reactions are considerably slower in the mixing region between the jets of fuel and air, leading to a smooth rise in temperature during the consumption of methane. This effect might lead to a better understanding of the interaction between chemistry and thermal radiation.

REFERENCES

Carvalho, M.G., Farias, T., and Fontes, P. (1991) Predicting radiative heat transfer in absorbing, emitting, and scattering media using the discrete transfer method. *ASME HTD*, **160**(17), 17–26.

Denison, M.K. and Webb, B.W. (1995) The spectral line-based weighted-sum-of-gray-gases model in non-isothermal non-homogeneous media. *J. Heat Trans.*, **117**, 359.

Eaton, A.M., Smoot, L.D., Hill, S.C., and Eatough, C.N. (1999) Components, formulations, solutions, evaluations, and application of comprehensive combustion models. *Prog. in Ener. Combust. Sci.*, **25**, 387.

Fairweather, M. and Woolley, R.M. (2004) First-order conditional moment closure modeling of turbulent, non-premixed methane flames. *Combust. Flame*, **138**, 3.

Fluent Inc. (1997) Fluent User's Guide. New Hampshire, Inc., Lebanon, NH.

Garréton, D. and Simonin, O. (1994) Aerodynamics of steady state combustion chambers and furnaces. In *ASCF Ercoftac Cfd Workshop*, Org: EDF Chatou, France.

Guo, Z.M., Zhang, H.Q., Chan, C.K., and Lin, W.Y. (2003) Presumed joint probability density function model for turbulent combustion. *Fuel*, **82**, 1091.

Hottel, H.C. and Sarofim, A.F. (1967) Radiative Transfer, McGraw-Hill Book Company. New York.

Kuo, K.K. (1996) Principles of Combustion. John Wiley & Sons Inc., New York.

Launder, B.E. and Spalding, D.B. (1972) Mathematical Model of Turbulence Academic Press Inc., San Diego, CA.

Launder, B.E. and Sharma, B.I. (1974) Application of the energy-dissipation model of turbulence to the calculation of flow near a spinning disc. *Lett. Heat Mass Trans.*, **19**, 519.

Magel, H.C., Schnell, U., and Hein, K.R.G. (1996a) Modeling of hydrocarbon and nitrogen chemistry in turbulent combustor flows using detailed reactions mechanisms. In *3rd Workshop on Modeling of Chemical Reaction Systems*, The Combustion Institute, Heidelberg, 1–10.

Magel, H.C., Schnell, U., and Hein, K.R.G. (1996b) Simulation of detailed chemistry in a turbulent combustor flow. *Proc. Combust. Instit.*, **26**, 67.

Magnussen, B.F. and Hjertager, B.H. (1976) On mathematical models of turbulent combustion with special emphasis on soot formation and combustion. *Proc. Combust. Instit.*, **16**, 719.

Malikov, G.K., Lisienko, V.G., Malikov, K.Y., and Viskanta, R. (2002) A mathematical modeling and validation study of NOx emissions in metal processing systems. *ISIJ Inter.*, **42**, 1175–1181.

Miroslav, S., Stevanovic, Z, and Belosevic, S. (2001) Modeling of non-confined turbulent flow of two coaxial streams under combustion conditions. *Nonlinear Sciences Threshold Third Millenium*, **8**, 981.

Modest, M.F. and Zhang, H. (2002) The full-spectrum correlated-K distribution for thermal radiation for molecular gas particulate mixtures. *J. Heat Transf.*, **124**, 30.

Nieckele, A.O., Naccache, M.F., Gomes, M.S.P., Carneiro, J.E., and Serfaty, R. (2001) Evaluation of models for combustion processes in a cylindrical furnace. In ASME-IMECE, *International Conference of Mechanical Engineering* New York.

Nikuradse, J. (1933) Strömusgsgesetze in Rauhen Rohren. Forsch. Arb. Ing. – Ees.

Özisik, M.N (1985) Heat Transfer, McGrawHill Book Company, New York.

Salvador, S., Commandré J.M., and Kara Y. (2006) Thermal recuperative incineration of VOCs: CFD modeling and experimental validation. *Appl. Therm. Eng.*, **26**, 2355–2366.

Siegel, R. and Howell, J.R. (2002) Thermal Radiation Heat Transfer, Taylor & Francis Inc. New York.

Sika, P. (1992) Evaluation of direct-exchange areas for a cylindrical enclosure. *J. Heat Trans (ASME)*, **113**, 1040.

Smith, T.F., Shen, Z.F., and Friedman, J.N. (1982) Evaluation of coefficients for the weighted sum of gray gases model. *J. Heat Trans. (ASME)*, **104**, 602.

Spalding, D.B. (1979) Combustion and Mass Transfer, Pergamon Press Inc. New York.

Turns, S.T. (2000) An Introduction to Combustion — Concepts and Applications, McGraw-Hill Book Company, New York.

Van Wylen, G.J., Sonntag, E.R., and Bornake, C. (2003) Fundamentals of Classical Thermodynamics, John Wiley & Sons Inc. New York.

Yang, W. and Blasiak, W. (2004) Numerical study of fuel temperature influence on single gas jet combustion in highly preheated and oxygen deficient air. *J. Ener.*, **30**, 385.

Zhou, L.X., Qiao, L., Chen, X.L., and Zhang, J. (2002) A USM turbulence-chemistry model for simulating NOx formation in turbulent combustion. *Fuel*, **81**, 1703.

Zhou, L.X., Wang, F., and Zhang, J. (2003) Simulation of swriling combustion and no formation using a USM turbulence-chemistry model. *Fuel*, **82**, 1579.